Determining forward speed from accelerometer jiggle in aquatic environments

David E. Cade[1,*], Kelly R. Barr[1,4], John Calambokidis[2], Ari S. Friedlaender[3,5], Jeremy A. Goldbogen[1]

[1] *Department of Biology, Hopkins Marine Station, Stanford University, Pacific Grove, CA 93950, USA.*

[2] *Cascadia Research Collective, 218 1/2 W. 4th Avenue, Olympia, WA 98501, USA*

[3] *Marine Mammal Institute, Hatfield Marine Science Center, Department of Fish and Wildlife, Oregon State University, Newport, OR 97365, USA*

[4] *Present address: Center for Tropical Research, Institute for the Environment and Sustainability, Department of Ecology and Evolutionary Biology, University of California, Los Angeles, Los Angeles, CA 90095, USA*

[5] *Present address: Institute of Marine Sciences, University of California Santa Cruz, Santa Cruz, CA, 95064, USA*

**Author for correspondence: davecade@stanford.edu*

Key-words

Speed, accelerometer, flow noise, tag jiggle, biologging

Summary Statement

Cade and colleagues show that aquatic animal speed correlates exponentially with high frequency accelerometer motion in underwater animal-attached devices, and this motion can thus be used as a speed metric.

List of Abbreviations

CATS- Customized Animal Tracking Solutions

CI- Confidence Interval

OCDR- Orientation Corrected Depth Rate

PI- Prediction Interval

RMS- Root-mean-square

Abstract

How fast animals move is critical to understanding their energetic requirements, locomotor capacity, and foraging performance, yet current methods for measuring speed via animal-attached devices are not universally applicable. Here we present and evaluate a new method that relates forward speed to the stochastic motion of biologging devices since tag jiggle, the amplitude of the tag vibrations as measured by high sample rate accelerometers, increases exponentially with increasing speed. We successfully tested this method in a flow tank using two types of biologging devices and tested the method *in situ* on wild cetaceans spanning ~3 to >20 m in length using two types of suction cup-attached and two types of dart-attached tag. This technique provides some advantages over other approaches for determining speed as it is device-orientation independent and relies only on a pressure sensor and a high sample rate accelerometer, sensors that are nearly universal across biologging device types.

Introduction

The forward speed of an organism is a fundamental link between physiology, energy expenditure and ecology across a wide range of spatial and temporal scales (Tucker, 1970), yet accurately and consistently measuring speed in natural environments has proven difficult. An accurate understanding of speed reflects an animal's locomotor performance (Domenici, 2001), energetic costs (Claireaux et al., 2006; Clark et al., 2010; Videler, 1993; Watanabe et al., 2011), behavioral state (Aoki et al., 2012; Goldbogen et al., 2006) and also aids in 3D track reconstructions (Laplanche et al., 2015; Wilson and Wilson, 1988). In terrestrial environments, speed can be measured accurately using georeferencing techniques (e.g. von Hünerbein et al., 2000; Weimerskirch et al., 2002). However, global positioning systems (GPS) do not work underwater, thus in aquatic environments forward speed must be measured using multi-sensor, animal-borne tags (Aoki et al., 2012; Fletcher et al., 1996; Sato et al., 2003; Shepard et al., 2008; Wilson and Achleitner, 1985). While these devices have been successful in various contexts, all exhibit disadvantages including high-drag equipment (Kawatsu et al., 2009), orientation constraints (Chapple et al., 2015), a dependence on water clarity (Shepard et al., 2008), and unknown sensor responses within variable flow regimes (Wilson and Achleitner, 1985).

The most direct way to measure speed in aquatic environments is to measure an animal's change in depth when horizontal motion is small. If an animal's forward motion with respect to the horizontal plane is equivalent to its pitch, speed can be calculated from an orientation corrected depth rate (OCDR) (Miller et al., 2004) as:

$$OCDR = \Delta depth \cdot \sin(pitch)^{-1} \cdot \Delta time^{-1} \quad \text{(Eqn 1)}$$

However, this metric can only be relied on when pitch is accurately determined and sufficiently steep, so these periods are commonly used to perform *in situ* calibrations for other speed metrics that can then be used to estimate speed for the duration of the device deployment (e.g. Blackwell et al., 1999; Goldbogen et al., 2006; Miller et al., 2016; Sato et al., 2003). One such method relies on the

observation that the amplitude of flow noise recorded by a hydrophone increases exponentially with speed (Finger et al., 1979). *In situ* flow noise measurements are typically regressed against OCDR at high pitch, and then the calibration curve is applied to the entire time series (e.g. Fletcher et al., 1996; Goldbogen et al., 2006; Simon et al., 2009). This method is limited by errors at high and low speed (Goldbogen et al., 2006), errors associated with imperfect regression relationships, and relies on devices with higher battery and memory requirements than other onboard sensors.

Here we describe an alternative speed estimation method that relies only on a pressure sensor and high sample rate accelerometers (> 40 Hz) which are now commonplace in animal-attached tags. Accelerometers have been deployed on swimming animals from diverse taxa including birds (Noda et al., 2016), cartilaginous fish (Gleiss et al., 2011), bony fish (Wright et al., 2014), cnidarians (Fossette et al., 2015), pinnipeds (Ydesen et al., 2014), and both small (Wisniewska et al., 2016) and large cetaceans (Goldbogen et al., 2006). When moving through a dense medium like water at speeds above ~1 m s^{-1}, an accelerometer will record the continuous jiggling motion that results from passing through a turbulent flow (Movies 1 & 2). We demonstrate the jiggle method using data from three types of multi-sensor tags deployed on cetaceans and also test the method in a flow tank. Our data suggest that in addition to broader applicability, the jiggle method is robust to tag orientation differences and has smaller regression associated error than the flow noise method.

Materials and methods

Jiggle Method

The jiggle method can be implemented using Matlab v2014a (www.mathworks.com) code included as supplementary materials. The method was developed from the observation that the amplitude of stochastic tag motion increases exponentially with increasing speed (Fig. 1), and this tag motion is measured continuously by the device's accelerometers. Accelerometers measure a combination of both specific (dynamic) and gravity-related (static) acceleration, but speed cannot be determined directly by integrating acceleration since small errors in calibration and tag orientation aggregate when integration of measured quantities is attempted, and because separating the two forms of acceleration is prone to error (Van Hees et al., 2013; Ware et al., 2016). Instead of estimating speed from acceleration, the jiggle method regresses the root-mean-square (RMS) amplitude of accelerometer motion along three axes against speed calculated using OCDR. We then use these regression equations to estimate speed for a given jiggle magnitude across the entire data set.

The accelerometer jiggle amplitude along each axis is calculated using the function TagJiggle.m by bandpass filtering the magnitude of the high-frequency accelerometer signal using a 128 point symmetric finite impulse response (FIR) filter. A band-pass filter was used for consistency across deployments with up to an 800 Hz sampling rate. However, since most energy in the signal was in the lower frequencies, a high-pass filter could be used for most applications. The most robust filter was determined experimentally. For general use, a 10 to 90 Hz band pass filter gives broadly consistent results but the upper limit should be less than the Nyquist frequency (half the sampling rate). The filtered vector is binned (default is ½ second) and centered on each sampling point, and the

accelerometer jiggle RMS amplitude (J) of each bin is calculated on a dB scale relative to the accelerometer units.

Like any device that estimates speed based on water movement around an animal, different locations of the device on the animal and the size/shape of the animal itself will lead to different flow conditions and different water velocities at each tag location (Fiore et al., 2017; Schetz and Fuhs, 1999). Thus, calibration in a flow tank is not solely sufficient for speed estimation using any currently existing method, and an *in situ* calibration must be performed for every deployment. The function SpeedFromRMS.m, which can also be used to calculate relationships for other speed metrics (e.g. flow noise), uses OCDR at high pitch angles (default |pitch| > 45°) as the known speed values, and allows the user to graphically adjust the default parameters to provide greater thresholds for pitch and depth to increase the accuracy of OCDR. The function also allows the user to exclude periods of high roll rate which, for large animals like the baleen whales in this study with body diameter of 3 m rolling at 40° s^{-1} (Segre et al., 2016), could potentially add to the overall speed experienced by the tag in a non-forward direction.

Biologging devices attached with suctions cups are periodically subject to sliding on the animal's body surface, and in the process the tag may adopt a new orientation. To account for this, SpeedFromRMS.m calculates a separate curve for each user-defined period of tag orientation within a deployment. For each section, the script calculates a coefficient of determination (R^2) and produces plots of jiggle RMS amplitude versus OCDR (Fig. 1A) as well as plots of time versus speed calculated from accelerometer jiggle, time vs. speed from OCDR, and time versus depth.

When deriving the regression equation, better R^2 are obtained by calculating OCDR across several sample points. Commonly one second bins are used (e.g. Miller et al., 2016; Sato et al., 2003), but the Matlab scripts allow for flexibility in bin size and the user could choose to match OCDR bin size with jiggle amplitude bin size. Although speed can be calculated from an exponential regression of the accelerometer jiggle along any individual axis or multiple (orthogonal) axes, better results were obtained using a multi-variate, exponential regression across all axes. SpeedFromRMS.m employs the Matlab function fitnlm.m with robust fitting options such that:

$$OCDR = a \cdot e^{b \cdot (c_1 \cdot J_X + c_2 \cdot J_Y + c_3 \cdot J_Z)} \quad \text{(Eqn 2)}$$

where a & b are exponential regression coefficients, J_X, J_Y, and J_Z are the jiggle amplitude of each axis, and c_1, c_2, and c_3 are restricted to the range [0 1] and represent the corresponding contributions of each axis to the overall regression equation. For each section of tag orientation, all five coefficients may vary. An R^2, the 95% confidence interval, and 68 and 95% prediction intervals for the resulting regression curve are calculated from standard exponential regression of J on OCDR, where:

$$J = c_1 \cdot J_X + c_2 \cdot J_Y + c_3 \cdot J_Z \quad \text{(Eqn 3)}$$

Finally, the regression equation is applied to J for all time points such that the resulting speed vector matches the length and sampling frequency of the original data (Figs 1-3).

In vitro *tests*

Utilizing suction cups designed for deployment on cetacean skin, we attached three types of CATS video tags (Cade et al., 2016; Goldbogen et al., 2017) with sampling rates of 40, 400 and 800 Hz and an Acousonde (Burgess, 2009) sampling at 400 Hz to the bottom of a recirculating flow tank (Movie 1) with an 18 cm x 18 cm cross-sectional area. The devices were exposed to known incrementally increasing flow rates of 0.3 m s^{-1} to 3.1 m s^{-1} for periods of one minute at each speed (Fig. S1). Data were collected with the tags positioned in four orientations: A) directly against the flow, B) directly with the flow, C) angled against the flow, and D) directly against the flow with only the front two suction cups attached (Fig. S2). The flow tank was controlled with a motor operating at known revolutions per minute (RPM) and the speed at each RPM setting was measured using a Höntzsch flowtherm NT flowmeter (www.hoentzsch.com/en/) at the location where the tag would be placed. The motor generated up to 0.12 m s^{-1} variation in flow speed at each RPM setting, so the median flow tank speed was regressed against the linearized mean of the corresponding RMS value of the accelerometer jiggle. Since the flow tank itself vibrated during the trials (Fig. S1B), the tag was also attached to the outside of the tank and the accelerometer jiggle was calculated at each speed. The amplitudes of the tank vibrations were linearly subtracted from the values recorded in the flow before regressions were calculated (Fig. S2).

The coefficient of determinations of the exponential relationships between accelerometer jiggle and flow tank speed (V_F) were calculated for each axis separately and for the overall magnitude of the three accelerometer axes at each of the four tag positions using a single variate version of Eqn 3:

$$V_F = a \cdot e^{b \cdot J} \quad \text{(Eqn 4)}$$

The correlations were run for J calculated from the accelerometer jiggle at various frequency ranges (Fig. S3) and this was used to determine both the range and axis that yielded the highest correlation coefficient.

In situ *tests*

The accelerometer jiggle method was tested using data from four tag types deployed on humpback whales (*Megaptera novaeangliae*), fin whales (*Balaenoptera physalus*), blue whales (*Balaenoptera musculus*) and Risso's dolphins (*Grampus griseus*) off the coast of California. All tags were deployed from a 6 m rigid-hull inflatable boat using a 6 m pole under NMFS permits #16111, #14534 or #14809 as well as institutional IACUC protocols. Suction cup tags were either CATS video tags or DTAGs (Johnson et al., 2009) and medium duration dart attached tags (Szesciorka et al., 2016) were either Acousondes with a custom modified base or modified TDR-10 tags (Wildlife Computers, Redmond, WA) with an attached accelerometer and additional pressure sensor from CATS (www.cats.is). Accelerometer sampling rates ranged from 40 Hz to 790 Hz. Animal pitch and roll were calculated for DTAG deployments using the DTAG tool kit (https://www.soundtags.org/dtags/dtag-toolbox/) and for CATS and Acousonde deployments using

custom Matlab scripts (Cade et al., 2016). Accelerometers for DTAGs, Acousondes, and CATS deployment mn161117-10 utilized a dynamic range of ± 2g, and remaining CATS deployments recorded at ± 4g.

Accelerometer jiggle amplitudes for 23 baleen whale deployments were calculated and regressed against OCDR at thirteen frequency ranges to determine which filtering range consistently gave the best results (Fig. S3). Using the 10-90 Hz frequency, forward speed was determined both with a univariate and multivariate regression on OCDR for 27 total deployments on all species. The R^2 from a single regression relationship for the whole deployment was compared to the weighted mean R^2 (mR^2) of each tag orientation section. Filtering at 10 Hz removed gravity-related acceleration signals associated with postural changes for our deployments (Sato et al., 2007), but higher frequency floors could also be employed without substantially reducing efficacy (Fig. S3, Movie 2). For deployments with hydroacoustic data (21 of the 27 overall deployments), speed was additionally calculated from the RMS amplitude of flow noise on the hydrophones (Goldbogen et al., 2006; Simon et al., 2009). The acoustic noise in the 66 to 94 Hz frequency band was calculated from one-second bins around each data point, and the RMS amplitude was regressed against OCDR using SpeedFromRMS.m. For most varieties of biologging device, an anti-aliasing, pre-digitization high-pass filter is applied to both acoustic and accelerometer data, in the case of acoustics specifically to reduce flow noise, so care must be taken to choose a frequency band that is not adversely affected by the filtering.

Results

The amplitude of tag jiggle predictably increased with forward speeds greater than ~1 m s^{-1} across all tag deployments and tag types. We confirmed the jiggle-speed relationship in laboratory experiments and we clarified the accelerometer axes and frequency ranges (10-90 Hz) that provided the most robust predictors of speed (Fig. S3, Eqn 2). The lower workable limit of the method was deployment- and tag-specific with a mean minimum detected speed of 0.9 ± 0.3 m s^{-1} (mean ± s.d.). At the upper limit, two deep-diving fin whales with dart-attached Acousondes regularly exceeded 7 m s^{-1} on steep descents to 300 m with no apparent limitations in the method. In comparison, a flow-noise method used previously in the same species was limited to less than 5 m s^{-1} because of clipping on the hydrophone (Goldbogen et al., 2006).

We observed a single case of accelerometer clipping that was not associated with the tag breaking the water-air interface (Movie 2). In this case, a humpback whale with a CATS video tag deployed near the animal's head, the dynamic range of the accelerometer was set to its minimum value. The tri-axial tag jiggle method filtered at 10-90 Hz as described above resulted in an upper detection limit of 6.2 m s^{-1}, but if we used a lower-amplitude 70-90 Hz frequency band on only the y-axis signal (which was perpendicular to gravity for the high-speed event) it reduced the effect of clipping on speed determination (Movie 2). In the Risso's dolphins, clipping was more common occurring in two of the four deployments with accelerometers set to ± 2 g for a total of 12.9 s out of 20.1 hours of tag data.

Among all tag deployments and tag types, the jiggle amplitude was correlated with OCDR regardless of whether our analysis included data from individual or multiple accelerometer axes. For most tags, the z-axis accelerometer data slightly improved results, but the z-axis performed poorly in dart-attached tags (Fig. S3). The highest correlations were found using a multi-variate exponential model that included data from all three accelerometer axes (Eqn 2). This method increased mR^2 by 0.11 ± 0.07 (n=27) over the use of the vector magnitude of the three axes. Contrary to the tags in the flow tanks, for which including frequencies above 50 Hz did not improve results, R^2 values of the correlation for *in situ* deployments improved across tag types by including frequencies up to ~90 Hz (Fig. S3). This result implies that while the method can be used with sample rates as low as 40 Hz, sampling at rates higher than 180 Hz will improve speed estimation.

In 16 of 21 deployments where speed was also calculated from flow noise, the jiggle amplitude had a stronger correlation with OCDR, resulting in smaller prediction intervals (95%PI 0.20 ± 0.28 m s^{-1} smaller), than flow noise. The average difference between mR^2 values for the 21 deployments was 0.07 ± 0.11. Across all 27 *in situ* deployments, mR^2 for the jiggle method was 0.82 ± 0.09, while mean mR^2 for the flow noise method was 0.76 ± 0.16. As a further test and comparison of these methods, we analyzed data from a CATS tag (sampling at 40 Hz) and a DTAG (250 Hz) deployed simultaneously on the same animal (Fig. 2). The four data streams were comparable in both amplitude and inflection for both high and low speed events. The CATS tag detached earlier than the DTAG, first sliding back near the flukes. The faster speeds traveled by the peduncle while oscillating were recorded on the CATS tag as a 1 m s^{-1} difference in speed between the two tags (Fig. 2).

Discussion

The method for determining speed from accelerometer jiggle has several notable improvements over previous methods (i.e. flow noise), but some limitations that were common to previous techniques persist. Specifically, our analyses suggest that the jiggle-speed method is: 1) resilient to changes in tag orientation, 2) combines multiple metrics (three accelerometer axes) into a single model (Eqn 2), 3) is less affected by ambient noises than the flow noise method (Fig. 3), 4) has a high theoretical maximum detection limit, 5) is calculated only from low-power sensors that already exist on most devices, 6) is not subject to signal attenuation from pre-digitization high-pass filtering, and 7) exhibits higher model coefficients of determination (compared to flow noise) in all tag deployments sampled higher than 50 Hz. In addition to the ubiquity of accelerometers, the jiggle method has some advantages over propeller-based speed sensors that are commonly analyzed at 1 Hz resolution (Miller et al., 2016; Sato et al., 2003), can stall at both high and low speeds, must be properly oriented in the flow, and, for deployments on animals in highly productive waters or who dive near the sediment, are subject to clogging with particulates.

Due to the potentially high dynamic range of accelerometers, the jiggle method could potentially provide additional and direct validation of the highest swimming speeds in apex predators like sailfish (10 m s^{-1}) (Marras et al., 2015), white sharks (11 m s^{-1}) (Martin and Hammerschlag, 2012) and pilot whales (9 m s^{-1}) (Aguilar Soto et al., 2008). Typical test deployments (e.g. Fig. 1) did not

approach the maximum measurable speed. For this example, a jiggle amplitude of 2 g would have correlated with a speed of 9.1 m s^{-1} (17.7 kn), and a full range amplitude of 4 g would have correlated with a speed of 11.0 m s^{-1}. These values are above the normal swim speeds of most marine mammals and fish (Block et al., 1992) and within the theoretical range of maximum speeds (10-15 m s^{-1}) for cavitation-free swimming for lunate-tailed fish and mammals (Iosilevskii and Weihs, 2008; Svendsen et al., 2016). Since clipping was more commonly observed in smaller animals we recommend increasing accelerometer range to ± 4 g for non-baleen whale deployments, though in some systems this may reduce the sensitivity.

The minimum detectable speed for the jiggle method of ~0.9 ms^{-1} captures the mean swimming speed of 87% of the species reviewed by Sato et al. (2007). To detect slower swim speeds using the jiggle method, however, multiple accelerometers with different sensitivities could be used within the same tag. Alternatively, a dedicated device such as a semi-rigid antenna or dome that would vibrate or exhibit omnidirectional displacement in flow could be more sensitive to lower-speed flows. Currently, lower swim speeds are best measured by propeller-based systems (e.g. Sato et al., 2003).

Like any process that relies on models to make predictions outside of the observed data, the jiggle method has error associated with extrapolation from regression. Nevertheless, two tags on the same animal gave nearly identical speeds using the jiggle method (Fig. 2), with a mean difference between tags for data below 20 m of 0.16 ± 0.14 m s^{-1}. Additionally, substantial variance in the regression is likely due to inaccuracies in the OCDR metric, particularly during active stroking periods when pitch may deviate from the direction of forward travel (e.g. a 45° pitch with a 10° offset from the actual direction of travel would result in OCDR errors of 19%). When speed was measured in the flow tank, jiggle amplitude was more tightly correlated with speed (mean R^2 values were 0.97 ± 0.02 at the frequency range and axis with the highest correlation).

A final implication of the accelerometer-speed relationship is that biologically relevant signals may be obfuscated by high frequency accelerometer sampling during high-speed events, and caution should be used when analyzing accelerometer signals (e.g. accelerometer jerk (Simon et al., 2012; Ydesen et al., 2014) and acoustic calls (Goldbogen et al., 2014)) that could occur simultaneously with high speed events. Additionally, animals that do not themselves experience forces above a typical accelerometer sensitivity of ± 2 g may nevertheless have datasets with clipped accelerometer readings due to tag jiggle at high speed, and these periods should be scrutinized to ensure that orientation estimation is not affected during these biologically important high-speed events. In conclusion, our analysis provides a greater ability to predict and understand these periods of high-amplitude accelerometer signals that have previously been treated as background noise (Saddler et al., 2017; Stimpert et al., 2015), and details a method for utilizing these signals to estimate animal speed over a considerable range of values.

Acknowledgements

DTAG deployments were conducted as part of the SoCal BRS project led by Brandon Southall and raw tag data were processed by Stacy DeRuiter, Alison Stimpert and Ann Allen. Thanks should also be extended to Elliott Hazen for his feedback on the multi-variate method.

Author Contribution Statement

JAG conceived the idea and DEC designed the methodology; JC, ASF, DEC and JAG collected the *in situ* data; KRB collected the *in vitro* data; DEC analyzed the data; DEC led the writing of the manuscript. All authors contributed critically to the drafts and gave final approval for publication.

Competing Interests

No competing interests declared.

Funding

DTAG deployments funded under grants from the Navy's Living Marine Resources Program and the Office of Naval Research Marine Mammal Program. Monterey Bay CATS tag deployments funded by grants from the American Cetacean Society Monterey and San Francisco Bay chapters, and by the Meyers Trust. Support for D.E.C. provided by Stanford University's Anne T. and Robert M. Bass Fellowship and for J.A.G. by the Office of Naval Research's Young Investigator Award (N00014-16-1-2477) and the National Science Foundation Integrative Organismal Systems award #1656691 and the Office of Polar Programs Antarctic Organisms and Ecosystems award #1644209.

Supporting Information/Appendices

Matlab code, Supplementary Figures, and two Movies can be found with this article online at:

References

Aguilar Soto, N., Johnson, M. P., Madsen, P. T., Díaz, F., Domínguez, I., Brito, A. and Tyack, P. (2008). Cheetahs of the deep sea: deep foraging sprints in short-finned pilot whales off Tenerife (Canary Islands). *Journal of Animal Ecology* **77**, 936-947.

Aoki, K., Amano, M., Mori, K., Kourogi, A., Kubodera, T. and Miyazaki, N. (2012). Active hunting by deep-diving sperm whales: 3D dive profiles and maneuvers during bursts of speed. *Marine Ecology Progress Series* **444**, 289-301.

Blackwell, S. B., Haverl, C. A., Boeuf, B. J. and Costa, D. P. (1999). A method for calibrating swim-speed recorders. *Marine Mammal Science* **15**, 894-905.

Block, B. A., Booth, D. and Carey, F. G. (1992). Direct measurement of swimming speeds and depth of blue marlin. *Journal of Experimental Biology* **166**, 267-284.

Burgess, W. C. (2009). The Acousonde: A miniature autonomous wideband recorder. *The Journal of the Acoustical Society of America* **125**, 2588-2588.

Cade, D. E., Friedlaender, A. S., Calambokidis, J. and Goldbogen, J. A. (2016). Kinematic Diversity in Rorqual Whale Feeding Mechanisms. *Current Biology* **26**, 2617-2624.

Chapple, T. K., Gleiss, A. C., Jewell, O. J., Wikelski, M. and Block, B. A. (2015). Tracking sharks without teeth: a non-invasive rigid tag attachment for large predatory sharks. *Animal Biotelemetry* **3**, 14.

Claireaux, G., Couturier, C. and Groison, A.-L. (2006). Effect of temperature on maximum swimming speed and cost of transport in juvenile European sea bass (Dicentrarchus labrax). *Journal of Experimental Biology* **209**, 3420-3428.

Clark, T. D., Sandblom, E., Hinch, S., Patterson, D., Frappell, P. and Farrell, A. (2010). Simultaneous biologging of heart rate and acceleration, and their relationships with energy expenditure in free-swimming sockeye salmon (Oncorhynchus nerka). *Journal of Comparative Physiology B* **180**, 673-684.

Domenici, P. (2001). The scaling of locomotor performance in predator–prey encounters: from fish to killer whales. *Comparative Biochemistry and Physiology Part A: Molecular & Integrative Physiology* **131**, 169-182.

Finger, R. A., Abbagnaro, L. A. and Bauer, B. B. (1979). Measurements of low-velocity flow noise on pressure and pressure gradient hydrophones. *The Journal of the Acoustical Society of America* **65**, 1407-1412.

Fiore, G., Anderson, E., Garborg, C. S., Murray, M., Johnson, M., Moore, M. J., Howle, L. and Shorter, K. A. (2017). From the track to the ocean: Using flow control to improve marine bio-logging tags for cetaceans. *PloS one* **12**, e0170962.

Fletcher, S., Le Boeuf, B. J., Costa, D. P., Tyack, P. L. and Blackwell, S. B. (1996). Onboard acoustic recording from diving northern elephant seals. *The Journal of the Acoustical Society of America* **100**, 2531-2539.

Fossette, S., Gleiss, A. C., Chalumeau, J., Bastian, T., Armstrong, C. D., Vandenabeele, S., Karpytchev, M. and Hays, G. C. (2015). Current-oriented swimming by jellyfish and its role in bloom maintenance. *Current Biology* **25**, 342-347.

Fournet, M. E., Szabo, A. and Mellinger, D. K. (2015). Repertoire and classification of non-song calls in Southeast Alaskan humpback whales (*Megaptera novaeangliae*). *The Journal of the Acoustical Society of America* **137**, 1-10.

Gleiss, A. C., Wilson, R. P. and Shepard, E. L. (2011). Making overall dynamic body acceleration work: on the theory of acceleration as a proxy for energy expenditure. *Methods in Ecology and Evolution* **2**, 23-33.

Goldbogen, J., Cade, D., Boersma, A., Calambokidis, J., Kahane-Rapport, S., Segre, P., Stimpert, A. and Friedlaender, A. (2017). Using Digital Tags With Integrated Video and Inertial Sensors to Study Moving Morphology and Associated Function in Large Aquatic Vertebrates. *The Anatomical Record* **300**, 1935-1941.

Goldbogen, J. A., Calambokidis, J., Shadwick, R. E., Oleson, E. M., McDonald, M. A. and Hildebrand, J. A. (2006). Kinematics of foraging dives and lunge-feeding in fin whales. *Journal of Experimental Biology* **209**, 1231-1244.

Goldbogen, J. A., Stimpert, A. K., DeRuiter, S. L., Calambokidis, J., Friedlaender, A. S., Schorr, G. S., Moretti, D. J., Tyack, P. L. and Southall, B. L. (2014). Using accelerometers to determine the calling behavior of tagged baleen whales. *The Journal of experimental biology* **217**, 2449-2455.

Iosilevskii, G. and Weihs, D. (2008). Speed limits on swimming of fishes and cetaceans. *Journal of the Royal Society Interface* **5**, 329-338.

Johnson, M., de Soto, N. A. and Madsen, P. T. (2009). Studying the behaviour and sensory ecology of marine mammals using acoustic recording tags: a review. *Marine Ecology Progress Series* **395**, 55-73.

Kawatsu, S., Sato, K., Watanabe, Y., Hyodo, S., Breves, J. P., Fox, B. K., Grau, E. G. and Miyazaki, N. (2009). A new method to calibrate attachment angles of data loggers in swimming sharks. *EURASIP Journal on Advances in Signal Processing* **2010**, 732586.

Laplanche, C., Marques, T. A. and Thomas, L. (2015). Tracking marine mammals in 3D using electronic tag data. *Methods in Ecology and Evolution* **6**, 987-996.

Marras, S., Noda, T., Steffensen, J. F., Svendsen, M. B., Krause, J., Wilson, A. D., Kurvers, R. H., Herbert-Read, J., Boswell, K. M. and Domenici, P. (2015). Not so fast: swimming behavior of sailfish during predator–prey interactions using high-speed video and accelerometry. *Integrative and comparative biology* **55**, 719-727.

Martin, R. A. and Hammerschlag, N. (2012). Marine predator–prey contests: ambush and speed versus vigilance and agility. *Marine Biology Research* **8**, 90-94.

Miller, P., Narazaki, T., Isojunno, S., Aoki, K., Smout, S. and Sato, K. (2016). Body density and diving gas volume of the northern bottlenose whale (*Hyperoodon ampullatus*). *Journal of Experimental Biology* **219**, 2458-2468.

Miller, P. J., Johnson, M. P., Tyack, P. L. and Terray, E. A. (2004). Swimming gaits, passive drag and buoyancy of diving sperm whales *Physeter macrocephalus*. *Journal of Experimental Biology* **207**, 1953-1967.

Noda, T., Kikuchi, D. M., Takahashi, A., Mitamura, H. and Arai, N. (2016). Pitching stability of diving seabirds during underwater locomotion: a comparison among alcids and a penguin. *Animal Biotelemetry* **4**, 10.

Saddler, M. R., Bocconcelli, A., Hickmott, L. S., Chiang, G., Landea-Briones, R., Bahamonde, P. A., Howes, G., Segre, P. S. and Sayigh, L. S. (2017). Characterizing Chilean blue whale vocalizations with DTAGs: a test of using tag accelerometers for caller identification. *Journal of Experimental Biology*, jeb. 151498.

Sato, K., Mitani, Y., Cameron, M. F., Siniff, D. B. and Naito, Y. (2003). Factors affecting stroking patterns and body angle in diving Weddell seals under natural conditions. *Journal of Experimental Biology* **206**, 1461-1470.

Sato, K., Watanuki, Y., Takahashi, A., Miller, P. J., Tanaka, H., Kawabe, R., Ponganis, P. J., Handrich, Y., Akamatsu, T. and Watanabe, Y. (2007). Stroke frequency, but not swimming speed, is related to body size in free-ranging seabirds, pinnipeds and cetaceans. *Proceedings of the Royal Society of London B: Biological Sciences* **274**, 471-477.

Schetz, J. A. and Fuhs, A. E. (1999). Fundamentals of fluid mechanics: John Wiley & Sons.

Segre, P. S., Cade, D. E., Fish, F. E., Potvin, J., Allen, A. N., Calambokidis, J., Friedlaender, A. S. and Goldbogen, J. A. (2016). Hydrodynamic properties of fin whale flippers predict maximum rolling performance. *Journal of Experimental Biology* **219**, 3315-3320.

Shepard, E. L., Wilson, R. P., Liebsch, N., Quintana, F., Laich, A. G. and Lucke, K. (2008). Flexible paddle sheds new light on speed: a novel method for the remote measurement of swim speed in aquatic animals. *ENDANGERED SPECIES RESEARCH* **4**, 157-164.

Simon, M., Johnson, M. and Madsen, P. T. (2012). Keeping momentum with a mouthful of water: behavior and kinematics of humpback whale lunge feeding. *The Journal of experimental biology* **215**, 3786-3798.

Simon, M., Johnson, M., Tyack, P. and Madsen, P. T. (2009). Behaviour and kinematics of continuous ram filtration in bowhead whales (*Balaena mysticetus*). *Proceedings of the Royal Society of London B: Biological Sciences* **276**, 3819-3828.

Stimpert, A. K., DeRuiter, S. L., Falcone, E. A., Joseph, J., Douglas, A. B., Moretti, D. J., Friedlaender, A. S., Calambokidis, J., Gailey, G. and Tyack, P. L. (2015). Sound production and

associated behavior of tagged fin whales (*Balaenoptera physalus*) in the Southern California Bight. *Animal Biotelemetry* **3**, 1.

Svendsen, M. B., Domenici, P., Marras, S., Krause, J., Boswell, K. M., Rodriguez-Pinto, I., Wilson, A. D., Kurvers, R. H., Viblanc, P. E. and Finger, J. S. (2016). Maximum swimming speeds of sailfish and three other large marine predatory fish species based on muscle contraction time and stride length: a myth revisited. *Biology Open* **5**, 1415-1419.

Szesciorka, A. R., Calambokidis, J. and Harvey, J. T. (2016). Testing tag attachments to increase the attachment duration of archival tags on baleen whales. *Animal Biotelemetry* **4**, 18.

Thompson, P. O., Cummings, W. C. and Ha, S. J. (1986). Sounds, source levels, and associated behavior of humpback whales, Southeast Alaska. *The Journal of the Acoustical Society of America* **80**, 735-740.

Thompson, P. O., Findley, L. T., Vidal, O. and Cummings, W. C. (1996). Underwater sounds of blue whales, Balaenoptera musculus, in the Gulf of California, Mexico. *Marine Mammal Science* **12**, 288-293.

Tucker, V. A. (1970). Energetic cost of locomotion in animals. *Comparative Biochemistry and Physiology* **34**, 841-846.

Van Hees, V. T., Gorzelniak, L., Leon, E. C. D., Eder, M., Pias, M., Taherian, S., Ekelund, U., Renström, F., Franks, P. W. and Horsch, A. (2013). Separating movement and gravity components in an acceleration signal and implications for the assessment of human daily physical activity. *PloS one* **8**, e61691.

Videler, J. J. (1993). Fish swimming: Springer Science & Business Media.

von Hünerbein, K., Hamann, H.-J., Rüter, E. and Wiltschko, W. (2000). A GPS-based system for recording the flight paths of birds. *Naturwissenschaften* **87**, 278-279.

Ware, C., Trites, A. W., Rosen, D. A. and Potvin, J. (2016). Averaged Propulsive Body Acceleration (APBA) Can Be Calculated from Biologging Tags That Incorporate Gyroscopes and Accelerometers to Estimate Swimming Speed, Hydrodynamic Drag and Energy Expenditure for Steller Sea Lions. *PloS one* **11**, e0157326.

Watanabe, Y. Y., Sato, K., Watanuki, Y., Takahashi, A., Mitani, Y., Amano, M., Aoki, K., Narazaki, T., Iwata, T. and Minamikawa, S. (2011). Scaling of swim speed in breath-hold divers. *Journal of Animal Ecology* **80**, 57-68.

Weimerskirch, H., Bonadonna, F., Bailleul, F., Mabille, G., Dell'Omo, G. and Lipp, H.-P. (2002). GPS tracking of foraging albatrosses. *Science* **295**, 1259-1259.

Wiggins, S. (2003). Autonomous acoustic recording packages (ARPs) for long-term monitoring of whale sounds. *Marine Technology Society Journal* **37**, 13-22.

Wilson, R. and Achleitner, K. (1985). A distance meter for large swimming marine animals. *South African Journal of Marine Science* **3**, 191-195.

Wilson, R. and Wilson, M.-P. (1988). Dead reckoning: a new technique for determining penguim movements at sea. *Meeresforschung* **32**, 155-158.

Wisniewska, D. M., Johnson, M., Teilmann, J., Rojano-Doñate, L., Shearer, J., Sveegaard, S., Miller, L. A., Siebert, U. and Madsen, P. T. (2016). Ultra-high foraging rates of harbor porpoises make them vulnerable to anthropogenic disturbance. *Current Biology* **26**, 1441-1446.

Wright, S., Metcalfe, J. D., Hetherington, S. and Wilson, R. (2014). Estimating activity-specific energy expenditure in a teleost fish, using accelerometer loggers. *Marine Ecology Progress Series* **496**, 19-32.

Ydesen, K. S., Wisniewska, D. M., Hansen, J. D., Beedholm, K., Johnson, M. and Madsen, P. T. (2014). What a jerk: prey engulfment revealed by high-rate, super-cranial accelerometry on a harbour seal (*Phoca vitulina*). *Journal of Experimental Biology* **217**, 2239-2243.

Figures

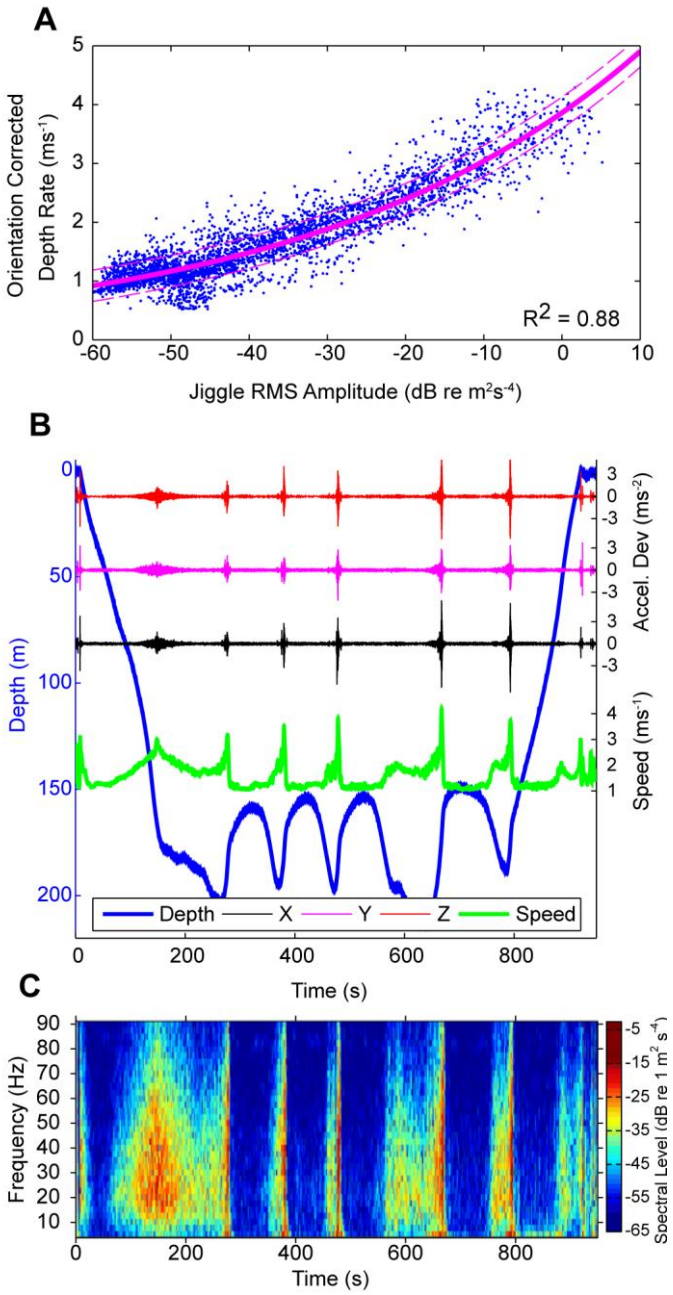

Fig. 1- Accelerometer jiggle during a blue whale (bw14_212a) feeding dive. (A) Jiggle amplitude regressed against periods of OCDR when |pitch| > 45° (B) Sampling at 250 Hz, the accelerometer signal in all three axes increases in amplitude during descent and ascent and preceding each lunge feeding event. Accelerometer signals are deviations from a 0.4 s running mean of each axis. Speed was smoothed with a one second running mean filter. (C) A 250 point FFT with 25% overlap of the y-axis accelerometer signal, calculated and displayed using Triton (Wiggins, 2003).

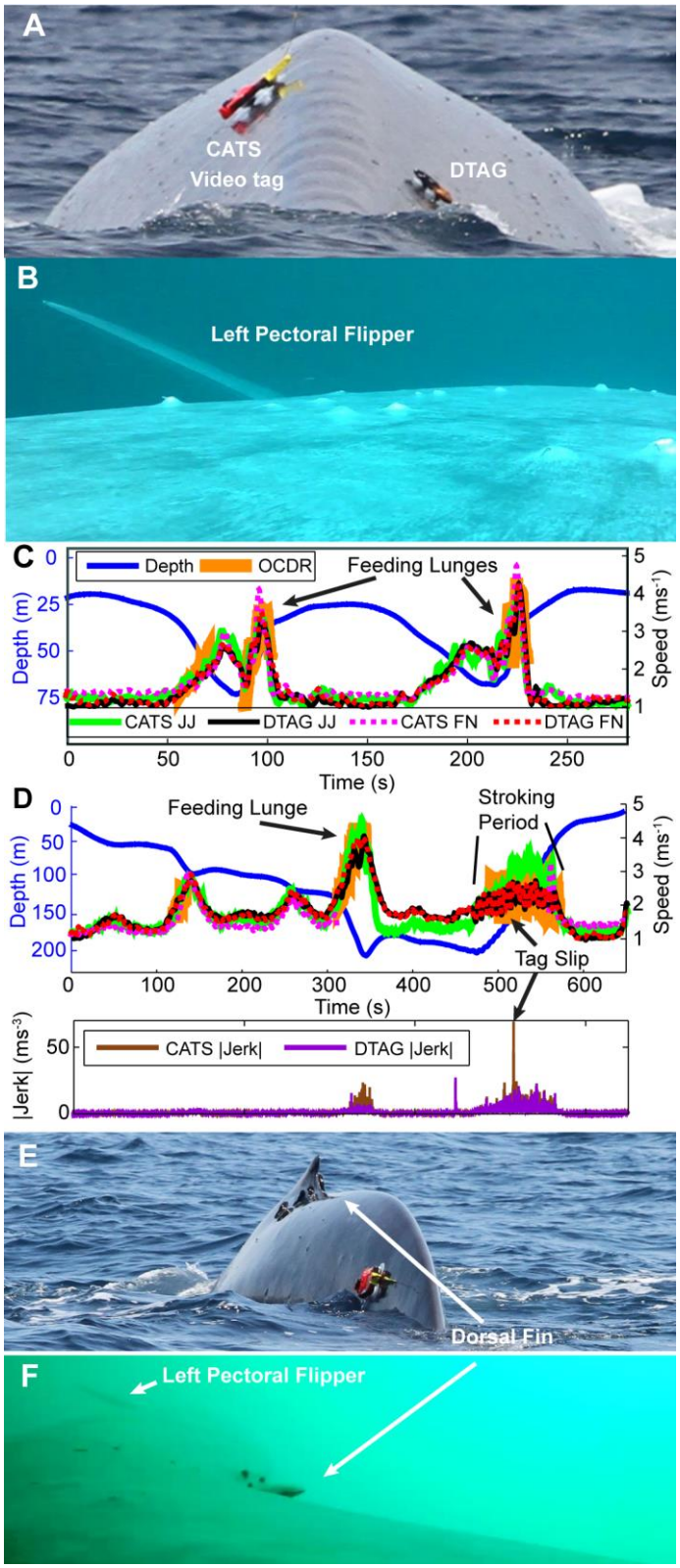

Fig. 2- Speed measurements from deployments of a CATS tag (bw140806-2) and a DTAG (bw14_218a) on a blue whale. A) Both tag locations. B) Video from CATS tag shows initial tag position near the pectoral flipper. C) Five metrics of animal speed (JJ = jiggle, FN = flow noise, OCDR = orientation corrected depth rate when |pitch| > 45°) smoothed with a 1 s running mean filter showing comparable magnitudes and inflections. D) The CATS tag slipped to the peduncle. The difference in amplitude of speed measured from the two tags reflects the increased peduncle motion

during fluking; at the conclusion of fluking the two metrics return to comparable values. OCDR during fluking is an unreliable metric of speed due to large oscillations when the travel direction does not coincide with animal pitch. The new position of the CATS tag is shown in E and in the tag video in F.

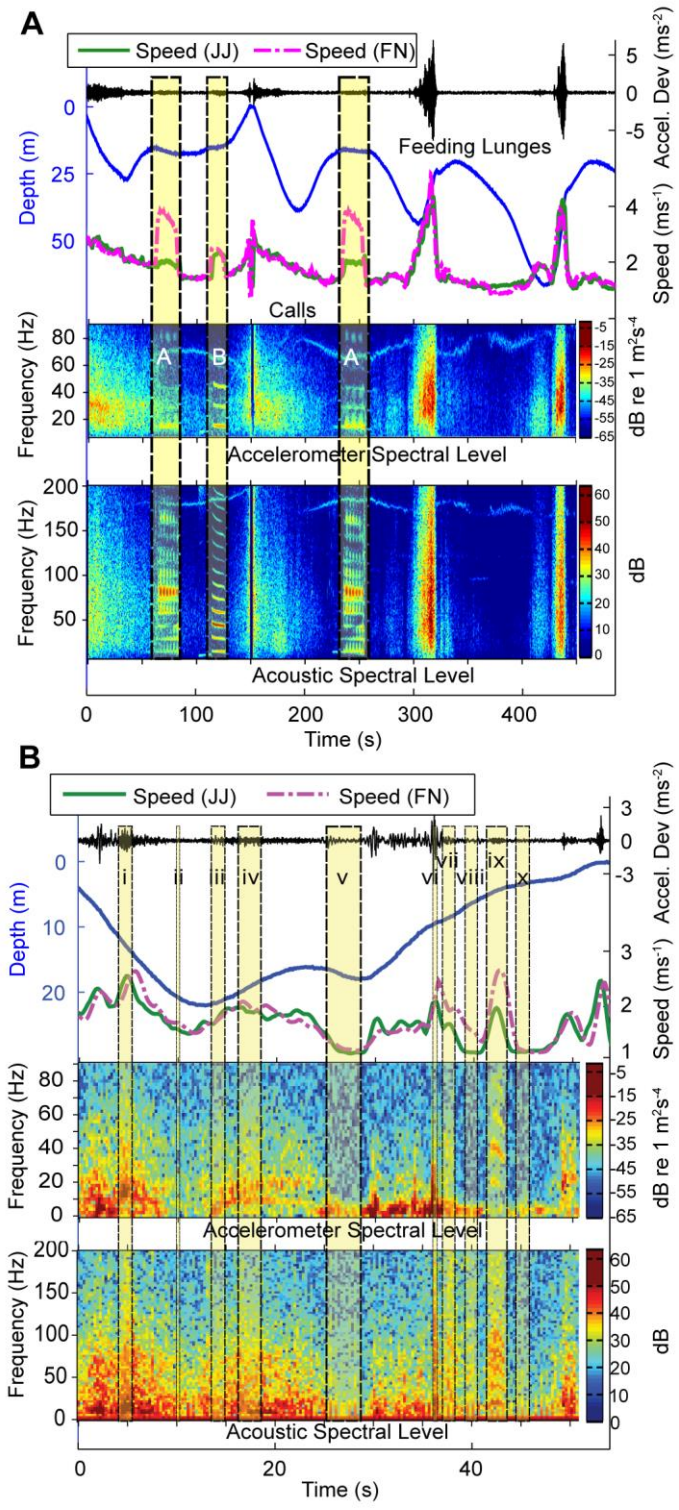

Fig. 3- Speed calculated from accelerometer motion and acoustic flow noise during the presence of other acoustic noise. Accel. Dev. is the z-axis deviation from a 0.4 s running mean of the accelerometer signal. JJ = jiggle, FN = flow noise. Spectrograms produced using *Triton*; dB values are self-referenced in the acoustic spectrograms. A) A blue whale (bw14_262b) with stereotypical A and B calls (Thompson et al., 1996) recorded on the hydrophone and the accelerometer. Type A calls had most of their acoustic energy in the harmonics that overlapped with the filtered frequencies and showed dramatic increases in flow noise-derived speed. Accelerometer spectrogram is a 250 point FFT with 25% overlap. Acoustic data were downsampled to 8 kHz, and displayed using a 7000 point

FFT with 25% overlap. B) A humpback whale (mn151012-7) with ten bioacoustic events. Events viii and ix were low-frequency vocalizations common to humpback whales in the NE Pacific (Fournet et al., 2015; Thompson et al., 1986). Event ix was apparent in both the accelerometer and hydrophone signal. Accelerometer spectrogram used a 200 point FFT with 50% overlap. Acoustic data were recorded at 22.05 kHz and are displayed using an 8192 point FFT with 25% overlap.

Fig. S1

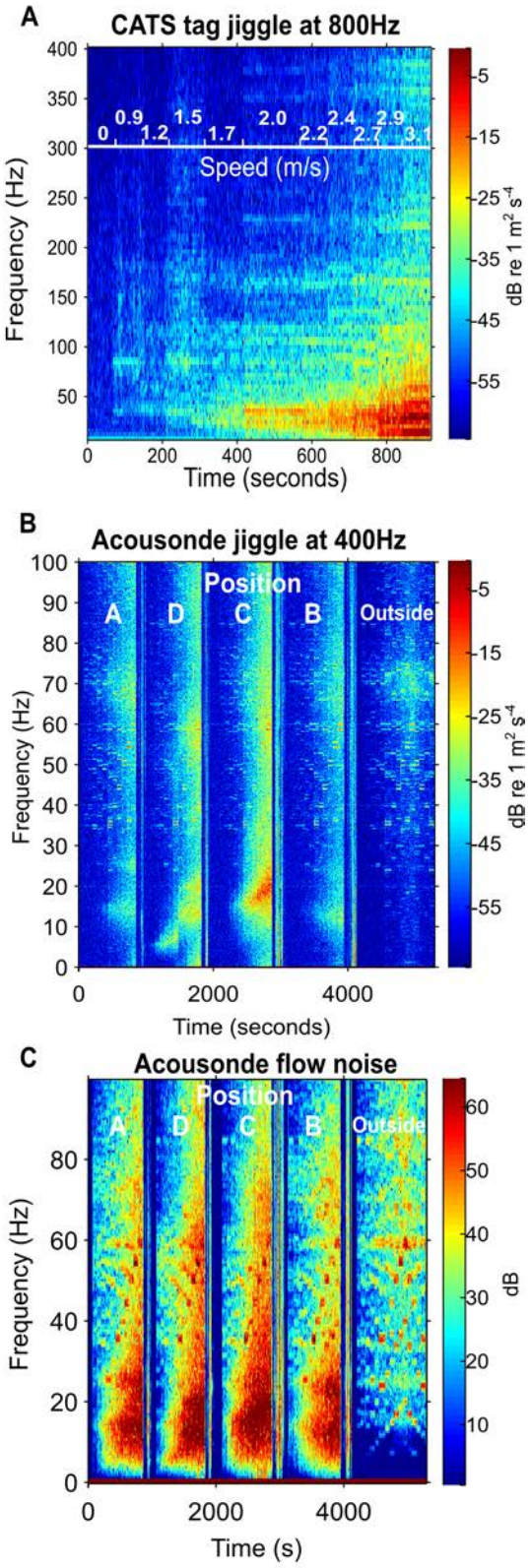

Fig. S1- Jiggle amplitude (A&B) and flow noise amplitude (C) for tags in a flow tank as functions of time and frequency as flow speed increases. Data in panels B & C were collected simultaneously. Position A-D refer to Figure 4. Spectrograms produced and spectral levels calculated using *Triton*; dB values are self-referenced in the acoustic spectrograms since the appropriate calibration transfer functions were unknown.

Fig. S2-

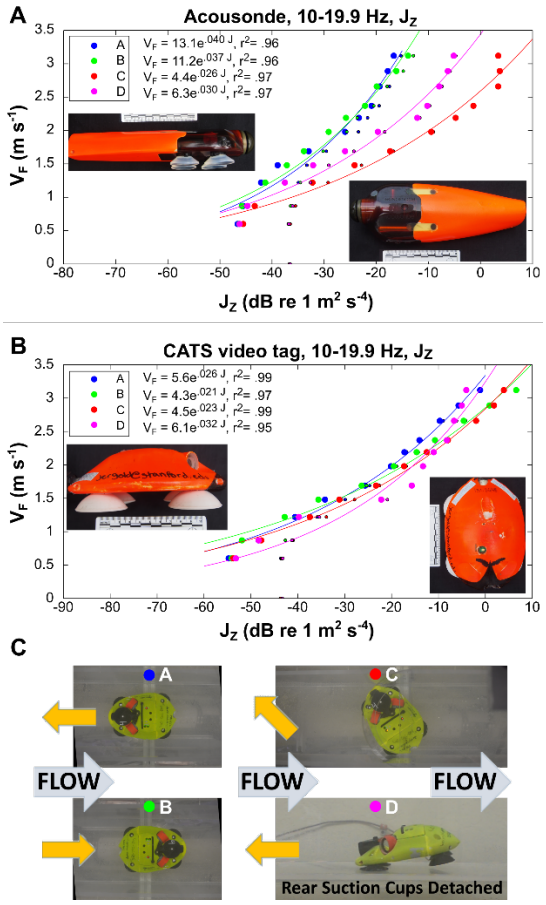

Fig. S2- Exponential regressions of accelerometer jiggle amplitude versus median flow speed in a recirculating flow tank for two tags in four different tag orientations. The Acousonde had larger variation in model coefficients for different tag orientations whereas the CATS tag, with a more symmetrical profile was more resilient to tag orientation differences. The tags are pictured with a 10 cm ruler for scale. A) Acousonde z-axis accelerometer jiggle. B) CATS tag (type m, see Cade *et al.* 2016) z-axis accelerometer jiggle. C) CATS tag (type p2) pictured in the four tested orientations, yellow arrows indicate the direction of the front of the tag. All plots show the jiggle calculated in the 10-19.9 Hz bandwidth. Small dots are calculated jiggle amplitudes while big dots (on which the regression was run) result from subtracting the jiggle amplitude associated with tank vibrations.

Fig. S3

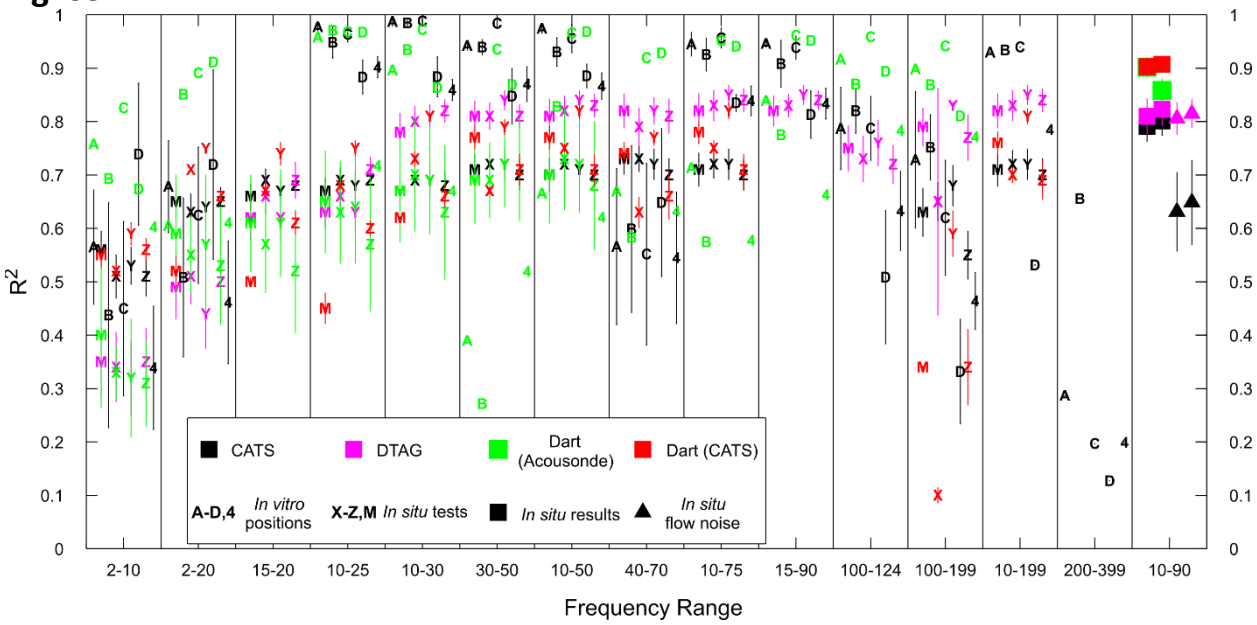

Fig. S3- Coefficients of determination (R^2) for calibration curves resulting from *in vitro* and *in situ* tests and the final results for 25 deployments (last column). A-D refer to different tag positions (Figure 3), 4 refers to a single calibration curve for all 4 positions. *In vitro* data shown is for curves regressing the magnitude of all three axes versus the median flow speed over a one minute period. X-Z are calibration curves from the jiggle in each axis separately, and M is the calibration curve for the magnitude of all three axes. Tag type are arranged by color. *In situ* results are only for baleen whale species.

Movies

Movie 1- A CATS video tag in the experimental flow tank. Z-axis motion is apparent.

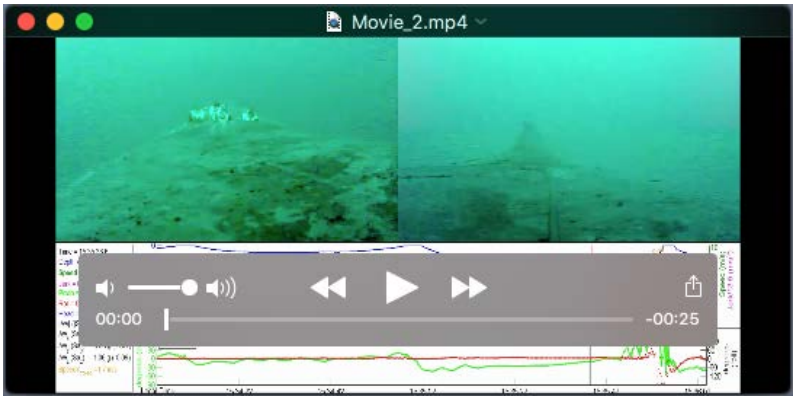

Movie 2- Multi-axis jiggling is apparent from camera motion during this deployment on a humpback whale (deployment mn161117-10) when the animal moves at high speed preceding a breach. Clipping of the accelerometer signal is apparent in the 10-90 Hz speed signal (green line), but if the jiggle signal is filtered at a higher frequency, the effect of clipping can be mitigated though not eliminated.